SUPPORTING MATERIAL

STED nanoscopy reveals molecular details of cholesterol- and cytoskeleton-modulated lipid interactions in living cells

V. Mueller[1], C. Ringemann[1], A. Honigmann[1], G. Schwarzmann[2], R. Medda[1], M. Leutenegger[1], S. Polyakova[1], V. N. Belov[1], S.W. Hell[1], C. Eggeling[1]

[1] Department of Nanobiophotonics, Max Planck Institute for Biophysical Chemistry, Am Fassberg 11, 37077 Göttingen, Germany. [2] LIMES Membrane Biology and Lipid Biochemistry Unit, University of Bonn, Gerhard-Domagk-Strasse 1, 53121 Bonn, Germany.

MATERIALS AND METHODS

Lipids

The structures of all synthesized lipids are depicted in Fig. S1.

Phosphoglycerolipids - phosphatidylethanolamine: **PE or PE-h**, *N*-(Atto647N)-1,2-dipalmitoyl-*sn*-glycero-3-phosphoethanolamine (head group labeling, Atto-Tec, Siegen, Germany). **PE-c**, phosphatidyl-ethanolamine-Atto647N (acyl chain replacement, synthesis see PE1 in (1)). **L-PE or L-PE-h**, *N*-(Atto647N)-1-palmitoyl-2-hydroxy-*sn*-glycero-3-phosphoethanolamine (Lyso-PE, Atto-Tec). **DOPE or DOPE-h**, *N*-(Atto647N)-1,2-dioleyl-*sn*-glycero-3-phosphoethanolamine (unsaturated acyl and alkyl chains, head group labeling, Atto-Tec).

Phosphoglycerolipids - phosphatidylcholine: **PC or PC-c**, Atto647N-phosphatidylcholine (acyl chain replacement, synthesized in the following steps: attachment of ω-(9-fluorenylmethyloxycarbonyl(FMOC)amino)dodecanoic acid to the free secondary hydroxy group of 1-octadecanoyl-*sn*-glycero-3-phosphorylcholine (Avanti Polar Lipids, Alabaster, AL) (3-nitro-1-[(2,4,6-triisopropylphenyl)sulfonyl]-1,2,4-tetrazole (TPSNT), *N*-methyl imidazole, CH_2Cl_2, room temperature), deprotection (5 % v/v piperidine in DMF, 0° - room temperature), and reaction with NHS-ester of Atto647N (DMF, Et_3N, room temperature)).

Sphingolipids – sphingomyelin: **SM-h**, Atto647N-*N*-lauroyl-*D-erythro*-sphingosyl-phosphorylethanolamine (Atto647N-ceramide-phosphorylethanolamine, head group labeling, Atto-Tec); **SM or SM-c**, *N*-(Atto647N)-sphingosylphosphorylcholine (*N*-Atto647-sphingomyelin, acyl chain replacement, Atto-Tec or synthesized in the following way: Atto647N-NHS-ester (1 mg, 2 µmol) and Lyso-SM (d18:1, sphingosylphosphorylcholine, Avanti, 1 mg, 2µmol) were combined in about 400 µl of dry DMF and 10 µl (69 µmol) of Et_3N were added. The mixture was stirred at room temperature overnight, DMF was evaporated in vacuum (ca. 1 mbar) and the product was isolated from the residue by HPTLC on SiO_2 plate (10×10 cm^2, 0.2 mm thick layer, VWR International) with $CHCl_3$:MeOH:H_2O (65:35:5, v:v:v) mixture as the mobile phase.). **L-SM or L-SM-h**, Atto647N-*D-erythro*-sphingosyl-phosphorylethanolamine (Lyso-SM, head group labeling, synthesized in the following way: *D-erythro*-sphingosyl-

phosphorylethanolamine (Sphingosyl PE (d18:1), Avanti, 3.2 mg, 7.6 µmol) dissolved in 1 ml $CHCl_3$-MeOH mixture (1:1) and Atto647N NHS-ester (1 mg, 1.2 µmol) were mixed at room temperature. After keeping the reaction mixture for 16 h at room temperature, the solvents were evaporated in vacuum (0.2-0.5 mbar), and the required mono-adduct was isolated by HPTLC using the solvent system $CHCl_3$:MeOH:H_2O (80:20:3)).

Sphingolipids – Ceramide: **Cer or Cer-c**, Atto647N-ceramide (acyl chain replacement, Atto-Tec). **GalCer**, Atto647N-galactosylsphingosine (acyl chain replacement, synthesized in the following way: psychosine (Sigma, 1 mg, 2.17 µmol) and Atto647N NHS-ester (1.45 mg, 1.72 µmol) were combined in dry DMSO (0.1 ml), and Et_3N (1 µl, 7 µmol) was added. The reaction mixture was stirred at room temperature for 7 h, evaporated in vacuum (0.2-0.5 mbar), and the product was isolated by preparative HPTLC using a $CHCl_3$:MeOH:H_2O (70:25:3) mixture and 10×10 cm HPTLC plate (VWR International)).

Sphingolipids – GM1-3: **GM1-h**, Atto647N-GM1 (head group labeling, synthesis see (1)); **GM1-c**, Atto647N-GM1 (acyl chain replacement, synthesis see (1)). **GM1-c2**, Atto647N-GM1 (additional short acyl chain carrying the dye, synthesis see (1)). **GM2**, Atto647N-GM2 (acyl chain replacement, synthesized from Lyso-GM2 and Atto647N NHS-ester following the published procedures (2)). **GM3**, Atto647N-GM3 (acyl chain replacement, synthesized from Atto647N-NHS-ester, C18-D-*erythro*-sphingosine (3) and monosialolactose from cow colostrum (4). Briefly, for the synthesis of the required lyso-GM3, sphingosine was protected and converted into (2*S*,23*R*,4*E*)-3-*O*-benzoyl-2-dichloroacetamido-4-octadecen-1,3-diol (5) and monosialolactose was protected and activated to nona-*O*-acetyl-α-monosialolactosyl bromide sialoyl-II^2-lactone essentially as described for monosialogangliotetraose (6). Both the protected sphingosine and activated monosialolactose were condensed in the presence of mercury cyanide (2) to a protected lyso-GM3 which upon deprotection (6) and acylation yielded Atto647N-GM3).

Phosphatidylinositol: **PI**, Atto647N-1,2-dioleoyl-*sn*-glycero-3-phosphorylinositol (head group labeling, synthesized in the following way: 1,2-dioleoyl-*sn*-glycero-3-phospho-(1'-myo-inositol) (ammonium salt) (18:1 PI, Avanti, 1.0 mg, 1.1 µmol) was dissolved in water (2 ml) and treated with the strong ion-exchange resin (Amberlite® IR-120) charged with sodium ions. Afterwards, the solution was lyophilized and the sodium salt of the lipid was dissolved in dry DMF (0.5 ml). 43 µl of a DMF-solution containing TPSNT (0.57 mg, 1.5 µmol) was added to a solution of Atto647N-carboxylic acid (1 mg, 1.3 µmol) followed by a solution of *N*-methylimidazole (0.5 mg, 6 µmol) in 5 µl DMF. After stirring for 40 min at room temperature, the solution of the activated Atto647N-carboxylic acid was mixed with the lipid solution, and the reaction mixture was stirred for 24 h at room temperature. The solvent was evaporated in vacuum (0.2-0.5 mbar), and the residue was separated by HPTLC using a $CHCl_3$:MeOH:H_2O (85:13:2) mixture. The product was isolated from the lower blue band and purified once more using the solvent system $CHCl_3$:MeOH:H_2O (70:25:3). The Atto647N dye is bound with one of the hydroxyl groups of the inositol residue.).

Ceramide Phosphorylinositol: **CPI**, Atto647N-*D*-*erythro*-sphingosyl-phosphorylinositol (sphingosyl-PI, acyl chain replacement, synthesized in the following way: *D*-erythro-sphingosyl-phosphorylinositol (Avanti, 1 mg, 1.8 µmol) and Atto647N NHS-ester (1 mg, 1.2 µmol) were combined in dry DMF (0.5 ml) in the presence of *i*Pr_2NEt (20 µl) and left for two days at room temperature. After removal of the solvents in vacuum (0.2-0.5

mbar), the residue was applied onto a HPTLC plate (10×10 cm), and the title compound ($R_f \approx 0.7$) was isolated with a $CHCl_3$:MeOH:H_2O (65:35:5) solvent mixture.).

Determination of the molecular structure of Atto647N

The molecular structures of the fluorescent dye Atto647N has been determined previously (1). The structure as given in Fig S1 had been established by NMR spectroscopy applying the dye's carboxylate (Atto-Tec). The molecular formula had been determined by high resolution mass-spectrometry (electro spray ionization). The final structure had been elucidated by 2D NMR spectroscopy (H-H correlation in CD_3OD at 600 MHz) and by comparison with the spectra of the model compound with the known structural fragment.

Bead measurements

Fluorescent bead measurements (Fig. 1 *A*) were performed on 20 nm large crimson beads (Molecular Probes, Eugene, OR) immobilized on coverslips with poly-*L*-lysine (0.1% w:v in water, Sigma-Aldrich, Steinheim, Germany) slide adhesive solution and embedded in Mowiol.

Supported lipid bilayer

A single-component supported lipid bilayer (SLB) was used as a control for free Brownian lipid diffusion (Fig. 1 *A*). The SLB was prepared based on the procedure described by Chiantia et al. (7). Briefly, the lipid DOPC (1,2-dioleoyl-*sn*-glycero-3-phosphocholine, Avanti) and the fluorescent lipid (PE-h) analog were mixed in organic solvents (Chloroform/MeOH 3:1) at a lipid concentration of ~ 10 mg/ml. The concentration of the fluorescent lipid analogs was on the order of 0.1-0.01 mol%. 50 µl of the lipid stock solution were evaporated for 30 min under vacuum. The dry lipid film was slowly rehydrated with 50 µl buffer solution (150 mM NaCl, 10 mM HEPES) and resuspended by vigorous vortexing. A small aliquot (10 µl) of the suspension was further diluted in 140 µl of the same buffer solution and sonicated for 30 min at 35° C until the buffer-lipid solution had become transparent. This solution was filled into a microscopy chamber with plasma-cleaned (Femto-RF, Diener Electronic, Nagold, Germany) standard microscope cover glass. A small amount of $MgCl_2$ (to an end concentration of 3 mM) was added to force vesicle spreading and fusion and to initialize the bilayer formation. 30 min later, the sample was thoroughly rinsed and kept under buffer solution. Such bilayers were stable for several hours.

Supported lipid bilayer – phase separation

Ternary lipid bilayers (Fig. S6), which separated in macroscopic liquid-ordered (Lo) and liquid-disordered (Ld) phases, were prepared by vesicle fusion (see above) on freshly cleaved MICA support (7). The lipid composition of the SLBs was DOPC/brains/cholesterol in a molar ratio of 1/1/0.7 containing 0.1 mol% fluorescent lipid analogue. During vesicle deposition on the MICA support and the subsequent washing step the temperature was hold at 50° C. After washing, the SLB was allowed to slowly cool down to room temperature.

Cellular measurements

Mammalian PtK2 cells were prepared as previously described (1, 8). Briefly, they were seeded on standard glass coverslips (diameter 18 or 25 mm, no. 1 thickness) to a confluence of about 80 % and grown at 37° C in a water-saturated atmosphere of 5 % CO_2 in air. The human HeLa cell line was grown in DMEM Glutamax high glucose (Invitrogen) supplemented with 10 % FBS, 100 U/ml penicillin, 100 µg/ml streptomycin and 1 mM sodium pyruvate. As for the PtK2 cells, HeLa cells were seeded on standard glass coverslips to have a confluence of about 80 % on the day of experiments.

Incorporation of the fluorescent lipid analogs into the plasma membrane of the living cells was accomplished via Bovine Serum Albumin (BSA) complexes as described previously (1). Briefly, 100 nmol of the lipid stock solutions ($CHCl_3$/MeOH, 3:1) were dried under a stream of nitrogen. The dried lipids were dissolved in 20 µl of absolute ethanol and vortexed vigorously after addition of 1 ml of defatted BSA solution (100-200 µM, i.e., 10^{-4} M defatted BSA in Dulbecco's Modified Eagle Medium DMEM without phenol-red buffered with 10 mM HEPES). Addition of 9 ml HDMEM (HEPES + DMEM = HDMEM) resulted in a final concentration of 10-20 µM BSA and 0.2 % (v:v) ethanol depending on the lipid analog. Afterwards, cells were washed with HDMEM and incubated with BSA-lipid-complexes (5–500 nM depending on the lipid analog) on ice for 30 min, washed in cold HDMEM and in some cases (for example for all sphingomyelin lipids) incubated at 37° C for 4 min in HDMEM.

We analyzed the lipid dynamics by placing the focused beams on random positions in the lower plasma membrane facing the coverslip and completed all measurements before significant internalization or any morphological changes in the cell could occur. Control measurements of SM and PE on the upper plasma membrane resulted in similar observations. The measurement times were kept short (~ 15 s) to avoid biasing distortion of the correlation data due to infrequent transits of bright particles such as cell debris. The coverslips were mounted in a special microscope chamber (RC-40, Warner Instruments, Hamden, CT). This chamber together with an objective heater (Cell MicroControls, Norfolk, VA) allowed controlling the sample temperature. If not stated otherwise, we performed the measurements at 25° C in HDMEM. Temperature, however, did not play an important role for the observed lipid interactions. In contrast to the coefficient of free diffusion, which followed an Arrhenius behavior, the observed trapping characteristics did not change between 22° C and 37° C (Fig. S2). Correlation data were recorded with fluorescent lipid concentrations resulting in $N \approx 1–5$ fluorescent particles per detection volume for STED and $N \approx 50–300$ for confocal recordings. The values and errors of the given parameters resulted from at least 20 and up to 100 measurements on the same and different positions of the same as well as different cells and are given as the median and the standard deviation of the mean. We checked that the observation times were given by the focal transit times and not shortened due to photobleaching, by measuring at low enough excitation intensities (Fig. S3). Additional control experiments excluded biasing effects by the excitation or STED light due to photobleaching, heating or other (non-linear) effects, as described previously (1, 8). We excluded diffusion of non-integrated lipids (or dye tags) by control measurements in between the cells.

Drug treatments

Cholesterol depletion: The cells were either treated with 1 U/ml *Streptomyces spec*. COase (Sigma) in HDMEM (and washed afterwards in HDMEM) or with 10 mM ß-cyclodextrin (ß-CD) (Sigma) in HDMEM (without phenol red) for 30 min under culture conditions. The COase or ß-CD treatment was either performed before or after the insertion of the fluorescent lipid analogs into the plasma membrane (1).

Latrunculin B: Treatment with 1 µM Latrunculin B (Sigma-Aldrich, #L5288) for 5-30 min at 37° C under culture conditions.

Nocodazol: Treatment with 15 µM Nocodazol (Calbiochem #487928, Merck) for 3h at 37° C under culture conditions. For recovery, cells were washed and rested for 30 min at 37°C.

Jasplakinolide: Treatment with 0.4 µM Jasplakinolide (Calbiochem #420197, Merck) for 5 min at 37° C under culture conditions.

Cytochalasin: Treatment with 1-10 µM Cytochalasin (Calbiochem, #250255, Merck) for 30 min at 37° C under culture conditions.

Zaragoic acid A: Treatment with 5 µM Zaragoic acid A (Sigma-Aldrich, #Z2626) for 48 h at 37° C in serum staved medium.

Myriocin: Treatment with 25 µM Myriocin (Sigma-Aldrich, #M1177) for 48 h at 37° C under culture conditions followed by 14-18 h treatment with 25 µM Myriocin in serum depleted medium.

STED nanoscope

The STED nanoscope was based on a home-built confocalized microscope setup equipped with a 633 nm laser (80 ps pulse width, LDH -P-635, PicoQuant, Berlin, Germany) for excitation of Atto647N fluorescence. The STED beam was provided by a Titanium:Sapphire laser system (MaiTai, Spectra-Physics, Mountain View, CA) operating at 770–780 nm with a repetition rate of 76 MHz. The pulse timing of both lasers was adjusted using a home-built electronic delay unit, where the STED pulses served as the trigger master. The STED laser pulses were stretched to a pulse length of approximately 250-350 ps using a 30 cm optical SF6 glass rod and a 120 m long polarization maintaining single-mode fiber (AMS Technologies, Munich, Germany). Fluorescence excitation and collection was realized using an oil immersion objective (PLAPON 60×, *NA* = 1.42, Olympus, Japan; or HCXPLAPO *NA* = 1.4, Leica Microsystems). The laser beams were spatially overlaid and the fluorescence light filtered by appropriate (dichroic) filters (AHF Analysentechnik, Tübingen, Germany). The doughnut-shaped focal spot of the STED beam featuring a central zero intensity was produced by introducing a phase-modifying plate (RPC Photonics, Rochester, NY) into the beam path, imprinting on the wave front a helical phase ramp $\exp(i\varphi)$ with $0 \leq \varphi \leq 2\pi$. A $\lambda/4$-plate ensured circular polarization of the STED and of the excitation beam. Precise positioning of the laser foci in the sample and sample scanning was realized by a beam scanning device (mirror tilting system PSH 10/2, Piezosystem Jena, Jena, Germany) for lateral directions and an objective lens positioning system (MIPOS 250, Piezosystem Jena) for the axial direction. The fluorescence was descanned and coupled into a multi-mode fiber splitter (Fiber Optic Network Technology, Surrey, Canada) with an aperture size corresponding to 1.4× the magnified excitation spot. The 50:50 split fluorescence signal was then detected by two single-photon counting modules (avalanche photo diode

SPCM-AQR-13-FC, Perkin Elmer Optoelectronics, Fremont, CA) and the recorded fluorescence counts were further processed by a hardware correlator card (Flex02-01D, Correlator.com, NJ). The focal intensity distribution of the excitation and STED light were measured by scanning a scattering gold bead of 80 nm in diameter (gold colloid, En.GC80, BBinternational, Cardiff, UK) using a non-confocal detector (MP 963 Photon Counting Module, Perkin Elmer). The laser powers P were measured directly at the sample plane. Together with the full-width-at-half-maximum $FWHM$ of the focal laser intensity distribution ($\approx$ 250 nm for 633 nm) they allow for the calculation of the time-averaged intensity $I = P / [\pi(FWHM/2)^2]$ (usually ~15-25 kW/cm^2 stemming from P = 5–8 µW for the excitation light) and a pulse peak intensity $I_{peak} = I/(\tau_P f)$ with pulse width $\approx$ 250-350 ps and repetition rate f = 76 MHz for the STED light. Calibration of the diameter $d(P_{STED})$ of the effective focal fluorescence spots formed by a certain STED power P_{STED} was performed either by imaging 20 nm large fluorescence beads or by STED-FCS measurements of the fluorescent lipid analogs in supported lipid bilayers (Fig. 1 *A*).

Fluorescence correlation spectroscopy (FCS)

FCS analyses characteristic fluctuations $\delta F(t) = \langle F(t)\rangle - F(t)$ in the fluorescence signal $F(t)$ over the time t about an average value $\langle F(t)\rangle$ by calculating the second-order auto-correlation function $G(t_c) = 1 + \langle \delta F(t)\, \delta F(t+t_c)\rangle / \langle F(t)\rangle^2$ (9-11). Here, t_c represents the correlation lag time. Triangular brackets indicate time averages. Fluctuations in the fluorescence signal are for example caused by characteristic variations in the concentration of fluorescent molecules, which diffuse in and out of the effective detection area, and by transitions into and out of a dark (triplet) state. Following earlier work, the auto-correlation function taking into account diffusion dynamics, the dark (triplet) state population and other kinetics causing changes in the fluorescence brightness can be approximated by (1),

$$G(t_c)=1 + (1/N)\, G_D(t_c)\, G_T(t_c)\, G_K(t_c) \qquad \text{(S1)}$$

where N is the particle number (i.e., the mean number of fluorescent molecules in the detection volume, which is proportional to the concentration divided by the measurement volume (or area for two-dimensional samples)), $G_D(t_c)$ the correlation term covering diffusion, $G_T(t_c) = 1 + T_{1eq}/(1-T_{1eq}) \exp(-t_c/\tau_T)$ the correlation term covering the dark (triplet) state population (with the equilibrium fraction T_{1eq} of molecules in the dark triplet state, and the triplet correlation time τ_T, characterized by the triplet population and depopulation kinetics), and $G_K(t_c) = 1 + K \exp(-t_c/\tau_K)$ is an additional kinetic term with amplitude K and correlation time τ_K. At the excitation intensities applied, T_{1eq} and τ_T of the Atto647N label were approximately 0.1 and 5 µs, respectively, and fixed throughout the analysis. We observed no dependence of values of T_{1eq} and τ_T on the STED power. Furthermore, our analysis of all FCS data recorded for lipid dynamics of the Atto647N-labeled lipids in living cells had to include an additional kinetic term with amplitude K = 0.05–0.1 and correlation time τ_K = 50–150 µs. This kinetic term was independent on the levels of excitation and STED light and might stem from the population of an additional dark state or conformational fluctuations of the dye-lipid system leading to changes in the fluorescence brightness. Its amplitude increased with hydrophobic environment as observed by measurements on model membranes at different humidity.

The diffusion term includes the time it takes for a lipid to diffuse through the effective focal spot regarding the inhomogeneous intensity profile of the laser focus (or of the detection area) as well as possible heterogeneity in diffusion due to, for example, binding to less mobile or immobile membrane compounds. We applied two different approaches to parameterize deviations from normal diffusion.

Anomaly: Deviations from normal Brownian diffusion may be analyzed using the model of anomalous subdiffusion (10). Due to anomalous diffusion, the mean square displacement $\langle r \rangle^2$ of a molecule's diffusion is not linear with time, but follows a power law in time t, $\langle r \rangle^2 = 4\ D\ t^{\alpha}$, with an apparent (averaged) diffusion coefficient D and an anomalous diffusion exponent α. Denoted anomaly throughout, the inverse $(1/\alpha)$ describes the degree of hindered diffusion. While diffusion is free for $(1/\alpha) = 1$ and follows Brownian motion characterized by a constant D, $(1/\alpha) > 1$ characterizes anomalous subdiffusion; the larger $(1/\alpha)$ the more hindered the diffusion. In FCS, anomalous diffusion is treated by introducing the anomalous diffusion exponent α into the term expressing the diffusion dynamics (1, 10).

$$G_D(t_c) = (1 + (t_c/\tau_D)^{\alpha})^{-1} \qquad \text{with} \quad \tau_D = d^2 / (8 \ln 2\ D) \tag{S2}$$

Here, we only considered diffusion along the lateral direction, since the plasma membrane can be treated as a flat, two-dimensional sample. τ_D is the average transit time of a fluorophore with the apparent diffusion coefficient D through the focal detection area of diameter d. For free Brownian diffusion D is constant for different d and τ_D scales linearly with the focal area d^2. This is different for anomalous diffusion, where D varies with d^2 depending on the spatial and temporal characteristic of the process causing the anomaly (e.g., time span and size of a trap or dimension of an obstacle). In this case, D represents an average apparent value.

Both, the intensity profile of the laser spot, which establishes the fluorescence emission profile (at the excitation intensities applied we can safely assume a linear dependency of the fluorescence emission on the laser intensity) and the detection profile of the microscope (given by the point-spread function of the microscope objective and the transmission function of the confocal pinhole) determine the spatial profile of the effective focal spot. Eq. S2 assumes a Gaussian-intensity profile, which is a good approximation for confocal FCS experiments at low laser intensities. For very small focal spots created by STED, this assumption slightly deviated from the actual shape of the focal spots (12). Consequently, the analysis of the correlation data may show an anomaly artifact. However, this bias hardly influenced the correlation analysis in the case of hindered diffusion, because the focal passage was dominated by trapping, which for example resulted in values of $1/\alpha > 1.4$. These values exceeded by far the artifact due to non-Gaussian spot profiles where $1/\alpha \approx 1.1$ (as determined from measurements of purely freely diffusing lipids in SLBs).

Binding: A second approach is based on the fact that anomalous diffusion is caused by transient trapping due to binding of the diffusing molecule to a fixed or comparatively slow moving particle. Such reactions are described by the on/off kinetic of the binding process to an immobile complex in the diffusion path of the molecule with an effective encounter rate k_{on} and a dissociation rate k_{off}. If the trapping time $1/k_{off}$ is much longer

than the average time the freely diffusing molecule would spend in the observation focus, the diffusion is reaction-dominated and we can describe the correlation function by

$$G_D(t_c) = (1-B)(1+t_c/\tau_{Dfree})^{-1} + B\exp(-k_{off}t_c) \qquad \text{(S3)}$$

where τ_{Dfree} is the average focal transit time for free diffusion (with free diffusion constant D_{free}) and $B = k_{off} / (k_{off}+k_{on})$ is the fraction of bound molecules (8, 13). We usually fixed τ_{Dfree} to values $\tau_{Dfree} = d^2/(8 \ln 2\, D_{free})$ expected for a value of D_{free} that was estimated from measurements at large d.

SUPPORTING DISCUSSION

Dye dependence

We found no significant dependence of the nanoscale trapping on the labeling conditions. The dynamics of the fluorescent lipid analogs remained unchanged when labeling with Atto647N at the head group or by replacing the acyl chain. We had previously observed consistent diffusion characteristics when applying another lipophilic marker (14) or when labeling the head group with a very polar dye (1). However, using the very same polar dye for labeling at the water-lipid interface (i.e., by acyl chain replacement) had resulted in almost diminished trapping and a much faster diffusion, indicating a less tight membrane anchoring (1). Therefore, neither the label type nor the label position had a significant influence except if labeled with a polar dye at the acyl chain. This independence was surprising, because it revealed that only the polarity but not the bulkiness of the dye label introduced a bias on at least the observed trapping dynamics.

Comparison to other cells

The observed dynamical characteristics were not specific for the PtK2 cells. For example, we observed a similar difference in the dynamics of SM and PE and a similar dependence on cholesterol in other cells such as the human HeLa cell line (Fig. S5). Although the trapping of SM was similar, diffusion of PE and SM in HeLa cells was slightly slower ($D_{conf} \approx 0.3$ μm^2/s) than in PtK2 cells ($D_{conf} \approx 0.5$ μm^2/s) and we determined lower on- and off-rates of the transient complex (k_{on}, $k_{off} \approx 30$ s^{-1} compared to k_{on}, $k_{off} \approx 70$ s^{-1} in PtK2 cells).

Further treatments for cholesterol dependence

We used the drug Zaragozic acid (ZA) to further highlight the dependence on cholesterol. ZA partially reduces the cellular cholesterol content by acting as an inhibitor of sterol synthesis (15). Fig. S5 depicts our results obtained for SM and GM1 on PtK2 cells following ZA treatment, rendering a partial abolishment of complex formation for SM and hardly any influence on GM1, similar to COase treatment.

Further treatments for cytoskeleton dependence

Fig. S5 also confirms the dependence of the SM dynamics on the cellular cytoskeleton applying other drugs. Similar to Latrunculin B, treatments with Cytochalasin, which blocks the polymerization of actin (16), or with Jasplakinolide, which was reported to disrupt actin filaments *in vivo* (17), partially reduced the trapping strength of SM. A similar reduction was observed upon treatment by Nocodazole, which interferes with the polymerization of the microtubule network. Strikingly, trapping was recovered to its original extend after removal of the drug.

Treatments for sphingomyelin reduction

At last, we investigated the changes in nanoscale membrane dynamics of SM and GM1 upon addition of Myriocin, which is supposed to inhibit sphingosine biosynthesis (with no effect on cholesterol) and we thus expect a lowering of endogenous sphingomyelin and other sphingolipids in the plasma membrane to a certain extent (15). While trapping of SM was reduced that of GM1 remained almost unchanged.

SUPPORTING REFERENCES

1. Eggeling, C., C. Ringemann, R. Medda, G. Schwarzmann, K. Sandhoff, S. Polyakova, V. N. Belov, B. Hein, C. von Middendorff, A. Schonle, and S. W. Hell. 2009. Direct observation of the nanoscale dynamics of membrane lipids in a living cell. Nature 457:1159-U1121.
2. Schwarzmann, G., and K. Sandhoff. 1987. Lysogangliosides: Synthesis and use in preparing labeled gangliosides. Methods Enzymol 138:319-341.
3. Sarmientos, F., G. Schwarzmann, and K. Sandhoff. 1985. Direct evidence by carbon-13 NMR spectroscopy for the erythro configuration of the sphingoid moiety in Gaucher cerebroside and other natural sphingolipids. Eur J Biochem 146:59-64.
4. von Nicolai, H., H. E. Mueller, and F. Zilliken. 1978. Substrate-Specificity of Neuraminidase from Erysipelothrix-Rhusiopathiae. Hoppe Seyler´s Z Physiol Chem 359:393-398.
5. Albrecht, B., U. Puetz, and G. Schwarzmann. 1995. Synthesis of fluorescent and radioactive analogues of two lactosylceramides and glucosylceramide containing ß-thioglycosidic bonds that are resistant to enzymatic degradation. Carbohydr Res 276:289-308.
6. Schwarzmann, G., P. Hofmann, and U. Puetz. 1997. Synthesis of ganglioside GM1 containing a thioglycosidic bond to its labeled ceramide(s). A facile synthesis starting from natural gangliosides. Carbohydr Res 304:43-52.
7. Chiantia, S., N. Kahya, J. Ries, and P. Schwille. 2006. Effects of Ceramide on Liquid-Ordered Domains Investigated by Simultaneous AFM and FCS. Biophys J 90:4500–4508.
8. Ringemann, C., B. Harke, C. V. Middendorff, R. Medda, A. Honigmann, R. Wagner, M. Leutenegger, A. Schoenle, S. Hell, and C. Eggeling. 2009. Exploring single-molecule dynamics with fluorescence nanoscopy. New J Phys 11:103054.
9. Fahey, P. F., D. E. Koppel, L. S. Barak, D. E. Wolf, E. L. Elson, and W. W. Webb. 1977. Lateral Diffusion in Planar Lipid Bilayers. Science 195:305-306.
10. Schwille, P., J. Korlach, and W. W. Webb. 1999. Fluorescence correlation spectroscopy with single-molecule sensitivity on cell and model membranes. Cytometry 36:176-182.
11. Wawrezinieck, L., H. Rigneault, D. Marguet, and P. F. Lenne. 2005. Fluorescence correlation spectroscopy diffusion laws to probe the submicron cell membrane organization. Biophys J 89:4029-4042.
12. Kastrup, L., H. Blom, C. Eggeling, and S. W. Hell. 2005. Fluorescence Fluctuation Spectroscopy in Subdiffraction Focal Volumes. Phys Rev Lett 94:178104.
13. Michelman-Ribeiro, A., D. Mazza, T. Rosales, T. J. Stasevich, H. Boukari, V. Rishi, C. Vinson, J. R. Knutson, and J. G. McNally. 2009. Direct Measurement of Association and Dissociation Rates of DNA Binding in Live Cells by Fluorescence Correlation Spectroscopy. Biophys J 97:337–346.
14. Kolmakov, K., V. Belov, J. Bierwagen, C. Ringemann, V. Mueller, C. Eggeling, and S. Hell. 2010. Red-Emitting Rhodamine Dyes for Fluorescence Microscopy and Nanoscopy. Chemistry 16:158 - 166.

15. Lasserre, R., X. J. Guo, F. Conchonaud, Y. Hamon, O. Hawchar, A. M. Bernard, S. M. Soudja, P. F. Lenne, H. Rigneault, D. Olive, G. Bismuth, J. A. Nunes, B. Payrastre, D. Marguet, and H. T. He. 2008. Raft nanodomains contribute to Akt/PKB plasma membrane recruitment and activation. Nature Chemical Biology 4:538-547.
16. Lenne, P. F., L. Wawrezinieck, F. Conchonaud, O. Wurtz, A. Boned, X. J. Guo, H. Rigneault, H. T. He, and D. Marguet. 2006. Dynamic molecular confinement in the plasma membrane by microdomains and the cytoskeleton meshwork. EMBO J 25:3245-3256.
17. Bubb, M. R., I. Spector, B. B. Beyer, and K. M. Fosen. 2000. Effects of Jasplakinolide on the Kinetics of Actin Polymerization. J Biol Chem 275:5163–5170.
18. Baumgart, T., A. T. Hammond, P. Sengupta, S. T. Hess, D. A. Holowka, B. A. Baird, and W. W. Webb. 2007. Large-scale fluid/fluid phase separation of proteins and lipids in giant plasma membrane vesicles. PNAS 104:3165–3170.

SUPPORTING FIGURES

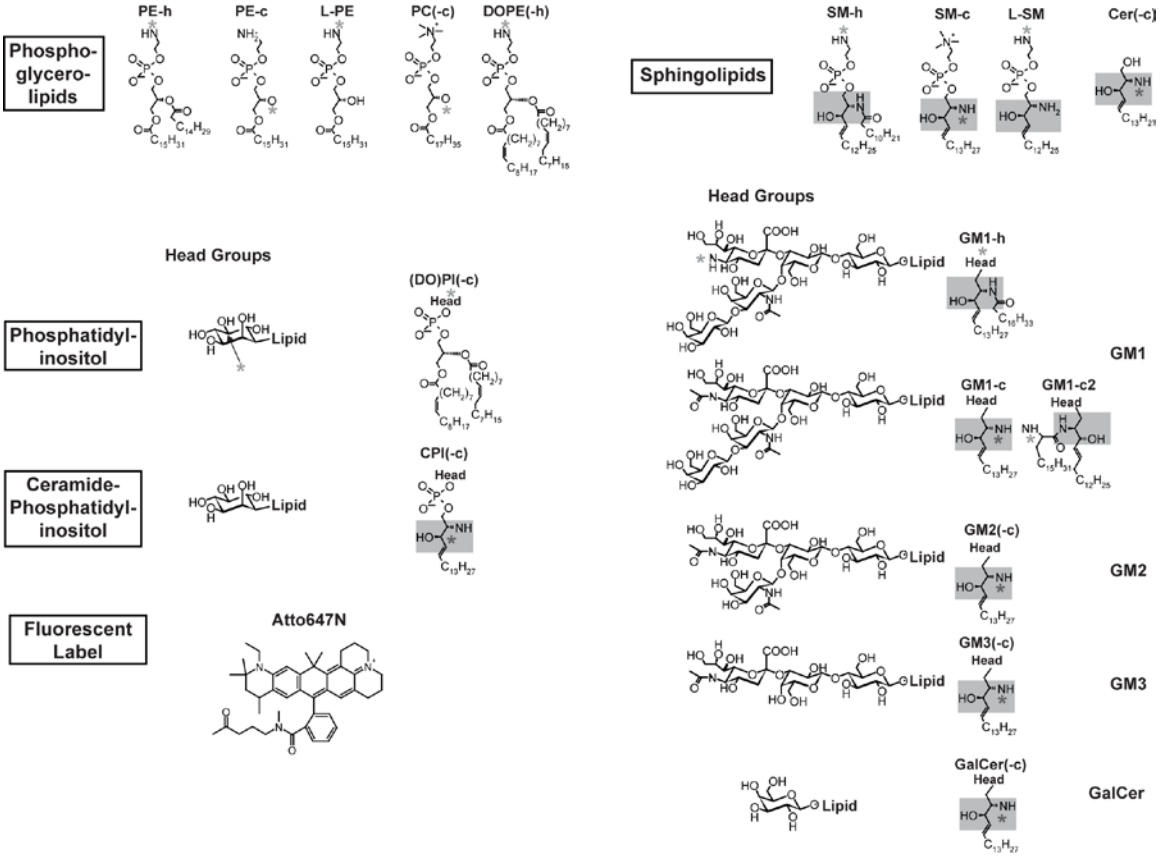

Figure S1. Structures of the fluorescent label and the fluorescent lipid analogs with the structural elements of ceramide (or sphingosine) that may participate in hydrogen bonding marked in grey. The asterix denotes the position of the fluorescent label Atto647N.

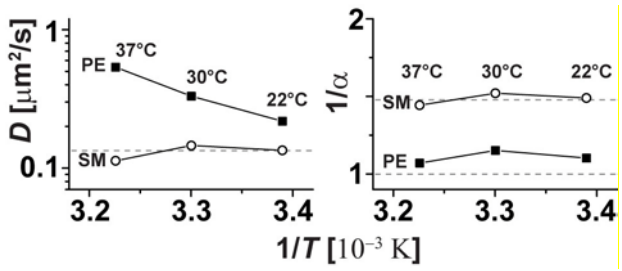

Figure S2. Dependence of the molecular trapping of SM on temperature. Diffusion coefficient *D* (left) and anomaly ($1/\alpha$) (right) of the STED recordings ($d \approx 40$ nm) of SM (white) and PE (black) for different sample temperatures *T*. Dashed lines highlight values of SM at 22° and ($1/\alpha$) = 1. While the apparent diffusion coefficient *D* of PE increased with temperature *T*, that of SM stayed constant. The Arrhenius behavior confirmed the (almost) free diffusion characteristics of the PE lipids in the plasma membrane. In contrast, the insensitivity of the SM dynamics on *T* demonstrated that temperature did not influence the formation of the lipid complexes, at least not in the measured temperature range of 22 to 37° C.

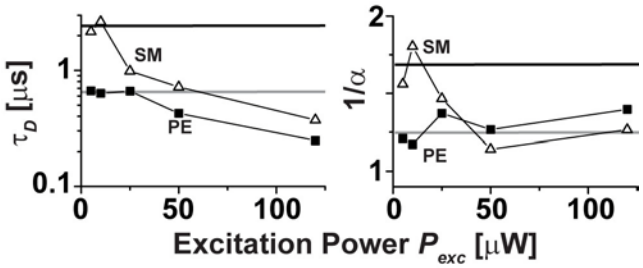

Figure S3. Dependence of the molecular dynamics of SM and PE on the excitation power P_{exc}: focal transit time τ_D (left) and anomaly ($1/\alpha$) (right) determined from FCS data of STED recordings (d = 40 nm). Increasing P_{exc} results in enhanced photobleaching and thus in an apparent reduction of τ_D due to irreversible loss of fluorescence before leaving the focal area. Molecules that are dwelling longer in the focal area are more probably photobleached. Consequently, with increasing P_{exc} trapped SM lipids are much less observed than freely diffusing SM and PE transits, resulting in the decrease of $1/\alpha$. We applied $P_{exc} \approx 10$ µW in all of our experiments, giving values of τ_D and ($1/\alpha$) highlighted by the grey and black lines.

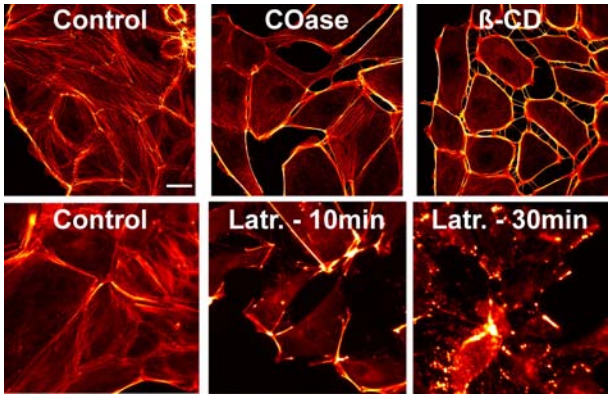

Figure S4. Scanning confocal images of PtK2 cells with labeled actin without (Control, left panels) and with COase, ß-CD and 10 min and 30 min Latrunculin B (Latr.) treatment. Morphological changes of the cells became apparent (stronger for ß-CD than for COase) as well as the modification of the actin network in the case of Latrunculin B. Cells were fixed after treatment for 10 min in 7% PFA, labeled with phalloidin-rhodamine to visualize the F-actin filaments and mounted in Mowiol. Scale bar 20 µm.

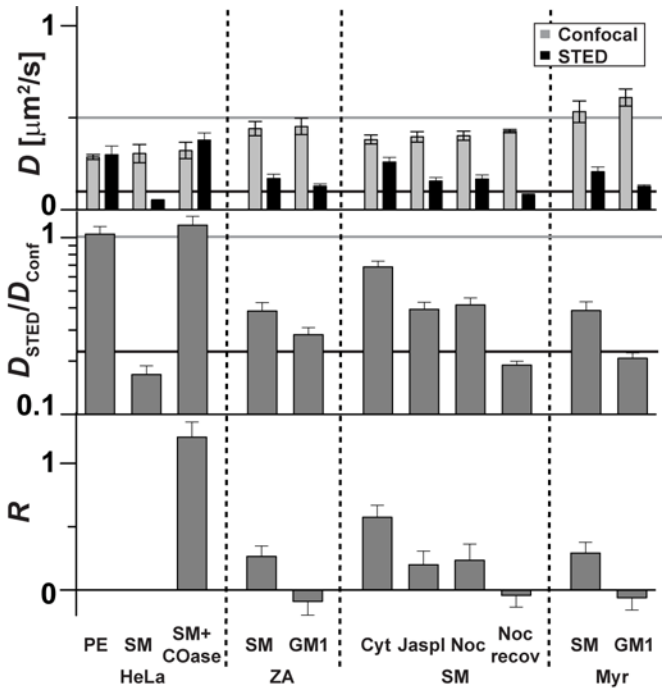

Figure S5. Dependence of the nanoscale trapping on various parameters. Apparent diffusion coefficient *D* (upper panel) determined from confocal (*d* = 240 nm, grey bars) and STED-FCS recordings (*d* = 40 nm, black bars), ratio D_{STED}/D_{conf} (middle panel) and recovery *R* (lower panel) for PE, SM and in some cases GM1: measurements in live HeLa cells (+COase: cholesterol depletion by COase), treatment by Zaragozic acid (ZA, lowering of the cholesterol level), Cytochalasin (Cyt, blocks the actin polymerization), Jasplakinolide (Jaspl, disruption of the actin filaments), and Nocodazol (Noc, blocking of the microtubule network polymerization, recov: recovery of the microtubule network after the drug removal), and Myriocin (Myr, reduction of the endogenous sphingomyelin).

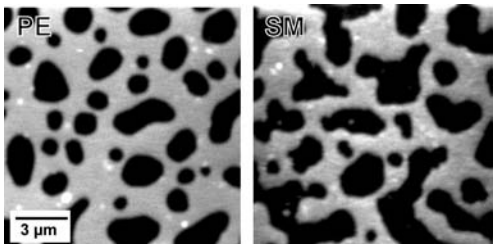

Figure S6. Scanning confocal images of a SLB with ternary DOPC/SM/CO lipid mixture incorporating the fluorescent PE (left) and SM (right) lipid analog. The signal level of detected fluorescence increases from black to white. The SLBs phase separated into a liquid-disordered Ld (white) and a liquid-ordered Lo phase (black). The Ld phase was highlighted by counterstaining with the liquid-disordered marker DiO (18) (data not shown). Clearly, in both cases, PE and SM, most of the signal stems from the Ld phase. Control experiments ruled out that the fluorescence of the lipid analogs was different in the two phases (e.g., quenched in the Lo phase). Therefore, partitioning into the Lo phase was low (partitioning coefficient $Kp < 0.03$) for both fluorescent PE and SM (as well as for GM1 – data not shown), in contrast to the almost complete Lo-partitioning expected for their natural counterparts. The partitioning coefficient $Kp = F(\mathrm{lo})/F(\mathrm{ld})$ was calculated by the ratio of fluorescence signal detected in the liquid ordered $F(\mathrm{lo})$ and in the liquid disordered phase $F(\mathrm{ld})$.